Heme Structure and Orientation in Single Monolayers of Cytochrome c on Polar and Nonpolar Soft Surfaces

Ann M. Edwards,* Ke Zhang,[†] C. Erik Nordgren,* and J. Kent Blasie*

*Department of Chemistry, University of Pennsylvania, Philadelphia, Pennsylvania 19104, and [†]Illinois Institute of Technology, Chicago, Illinois 60616 USA

ABSTRACT   Polarized x-ray absorption fine structure (XAFS) spectroscopy has been performed in fluorescence mode under total external reflection conditions on frozen hydrated single monolayers of yeast cytochrome c (YCC). The protein molecules were vectorially oriented within the monolayer by tethering their naturally occurring and unique surface cysteine residues to the sulfhydryl-endgroups at the surface of a mixed organic self-assembled monolayer, itself covalently attached to an ultrapure silicon wafer. The sulfhydryl-endgroups were isolated by dilution with either methyl- or hydroxyl-endgroups, producing macroscopically nonpolar or uncharged-polar soft surfaces, respectively. Independent information on the heme-plane orientation relative to the monolayer plane was obtained experimentally via optical linear dichroism. The polarized XAFS data have been analyzed both qualitatively and by a global mapping approach limited to systematically altering the various iron-ligand distances within a model for the local atomic environment of the heme prosthetic group, and comparing the theoretically generated XAFS spectra with those obtained experimentally. A similar analysis of unpolarized XAFS data from a frozen solution of YCC was performed using either the heme environment from the NMR solution or the x-ray crystallographic data for YCC as the model structure. All resulting iron-ligand distances were then used in molecular dynamics (MD) computer simulations of YCC in these three systems to investigate the possible effects of anisotropic ligand motions on the fits of the calculated to the experimental XAFS spectra.

INTRODUCTION

Accurate structural information on the active site of a peripheral membrane protein within a fully functional, vectorially oriented single monolayer on a soft surface is important to understanding the role of the protein-membrane interaction in the resulting structure-function relation for membrane proteins. For the electron transport peripheral membrane protein cytochrome c, the heme iron-ligand structure determines the prosthetic group's oxidation-reduction chemistry and, under physiological conditions, the axial ligands of the heme iron are the nitrogen from His(18) and the sulfur from Met(80). The sulfur ligand in particular plays a significant role in determining the structure and thermodynamic stability of the enzyme.

Previously, we have shown the ability to vectorially orient both peripheral and detergent-solubilized integral membrane proteins within a single monolayer by tethering the protein molecules to the endgroups of an organic self-assembled monolayer (SAM) chemisorbed onto the surface of a solid substrate by using designed specific interactions between particular residues on the protein's surface and the SAM's endgroups (Chupa et al., 1994). While other research groups have focused on measurements of the functional aspects of such (or closely related, e.g., Langmuir-Blodgett) monolayer systems that were not structurally

characterized (Song et al., 1993; Cullinson et al., 1994; Owaku et al., 1995; Jiang et al., 1996; Guo et al., 1996), we have focused instead on developing the physical techniques essential to determining the key structural features of the proteins within such vectorially oriented single monolayers. To date, this work has included both nonresonance and resonance x-ray diffraction (Pachence and Blasie, 1987; Pachence et al., 1989), optical linear dichroism (Pachence et al., 1990), and x-ray interferometry/holography (Blasie et al., 1992; Chupa et al., 1994; Edwards et al., 1997, 1998).

Polarized x-ray absorption fine structure (XAFS) spectroscopy can, in principle, provide extremely accurate measurements of metal-ligand bond lengths and orientations within the protein molecules in such vectorially oriented single monolayers. We have demonstrated this potential of polarized XAFS applied to such systems in order to obtain information on both the orientation of the protein with respect to the monolayer plane and the detailed atomic structure around the metal site(s) in the protein (Zhang et al., 1997; Edwards et al., 1999).

In this paper we have extended our work to monolayers of yeast cytochrome c (YCC) tethered to two very different soft organic surfaces—a nonpolar and an uncharged-polar surface. A modified experimental set-up has overcome the problems previously encountered due to radiation damage of the sample, enabling us to collect the first polarized XAFS data on frozen hydrated single monolayers that show significant differences depending on the plane of x-ray polarization relative to the monolayer plane and on the macroscopic nature of the soft surface. The spectra are also substantially different from the frozen solution spectrum of YCC. These data have been analyzed by comparison with

calculated spectra from a systematic variation of models for the local atomic environment of the heme prosthetic group based on either the NMR solution or x-ray crystallographic structure of YCC, and also from molecular dynamics (MD) computer simulations of these three different environments for YCC in order to allow for possible anisotropic ligand motions.

MATERIALS AND METHODS

XAFS spectroscopy about the iron K-absorption edge on single monolayers of a heme protein vectorially oriented on the soft surface of a SAM, itself chemisorbed onto a solid inorganic substrate, is technically challenging in the total external reflection geometry due to the low in-plane density of the heme iron atoms of interest. The silicon substrates, cleaved from 100-mm diameter, 0.4-mm-thick hyperpure polished Si(100) wafers (Wacker, Burghausen, Germany) to the desired size of $\sim 1 \times 3''$, were therefore soaked in 0.5 M EDTA (ethylenediaminetetraacetic acid, Sigma Chemical Co., St. Louis, MO) for 100–120 min, as this had previously been shown to reduce the surface iron content of the silicon still further (Zhang et al., 1997). They were then rinsed in ultrapure water (Millipore Corp., Bedford, MA) and dried. Substrates of 1-mm-thick silica (Esco products, Oak Ridge, NJ) were cut into $\sim 1 \times 2$ cm pieces for characterization of the protein monolayers by both polarized and unpolarized optical spectroscopy.

All substrates were cleaned and coated with the organic self-assembled monolayer (SAM) compounds following the general procedure of Sagiv (1980) with modifications that have been described previously (Xu et al., 1993; Edwards et al., 1997). Nonpolar surfaces were formed by a 6:1 ratio of dodecyltrichlorosilane (methyl-endgroup surface) and 11-trichlorosilylundecyl thioacetate (protected sulfhydryl-endgroup surface); while polar, but uncharged, surfaces were produced using a 6:1 ratio of trichlorosilylacetoxyundecane (protected hydroxyl-endgroup surface) and 11-trichlorosilylundecyl thioacetate (protected sulfhydryl-endgroup surface). The dodecyltrichlorosilane was purchased from Hüls (Piscataway, NJ). Details of the synthesis of the other organic compounds are given elsewhere (Wasserman et al., 1989; Edmiston et al., 1997). For both types of mixed monolayer surface, the protecting groups could be removed by immersing the coated substrate in a 50:50 mixture of methanol and concentrated hydrochloric acid (Fisher Scientific, Pittsburgh, PA) for 1.5 h to cleave them via acid hydrolysis, resulting in either macroscopically nonpolar or uncharged-polar surfaces containing isolated sulfhydryl functional endgroups. After rinsing well with ultrapure water, the activated surface was ready for immersion in a 10 μM solution of the protein, yeast cytochrome c from *Saccharomyces cerevisiae* in 1 mM TRIS, pH 8.0 (both from Sigma Chemical Co.). This protein exhibits a naturally occurring and unique surface cysteine residue 102 that would, therefore, be available for covalent disulfide bonding with the activated sulfhydryl endgroups of the SAMs. The specimens were incubated in the protein solution for ~ 24 h, then removed, rinsed several times in 1 mM TRIS buffer, pH 8.0, then placed in buffer for 45 min. This had previously been determined by unpolarized optical spectroscopy to be the optimal rinsing procedure to remove nonspecifically bound protein.

XAFS experiments were performed on the bending magnet beamline, X9-B at the NSLS in focusing mode. Focusing in the vertical direction was achieved by bending a nickel-coated mirror downstream and focusing in the horizontal direction by sagittal focusing of the second crystal of the monochromator. The sagittal focusing was adjusted during the scan. The fixed exit height, double crystal monochromator contained Si(111) crystals and the nickel-coated mirror was also used for harmonic rejection. The electron beam current was always between 150 and 300 mA during scans and the beam energy was 2.8 GeV. Energy calibration was achieved by scanning an iron foil and the energy resolution of the scan was estimated at ~ 2 eV.

The polarized XAFS experiments were performed in total reflection mode below the critical angle to maximize the signal and minimize the elastically scattered background (Zhang et al., 1997), with the incident angle determined by the distance between the direct and reflected beams at about two meters downstream from the sample. The silicon/SAM/protein samples were housed in a small chamber with polyvinylidene windows at the center of a Huber 4-circle diffractometer. The chi-circle was used to alter the angle between the plane of the single monolayer sample and the fixed horizontal plane of x-ray polarization, while the phi-circle was used to alter the angle of x-ray incidence on the sample. After removing excess buffer from the surface, one sample at a time was mounted on to a copper plate in the chamber by using a small amount of thermally conducting grease on the back of the silicon substrate. The temperature of the copper plate could be controlled by thermoelectric cooling elements and could be cooled to below 0°C in ~ 2 min. The temperature was then lowered to 263 K and was held constant here throughout the experiment to keep the sample hydrated and help prevent radiation damage. Dry nitrogen (in the case of the nonpolar SAM sample) or a mixture of dry nitrogen and dry helium (for the polar SAM specimen) was flowed gently through the chamber to remove the moist air and thereby prevent condensation on the sample chamber windows.

Ion chambers containing 100% nitrogen were placed before and after the sample chamber, the latter having an iron foil taped to its front window for energy calibration purposes during data analysis. Data were collected using a 13-element germanium detector (Canberra, Meriden, CT) at $\sim 90°$ to the incident x-ray beam. The detector was always operated within its linear regime (i.e., <80,000 incident counts per channel) and the full-width-half-maximum of the iron fluorescence peak indicated a resolution of 250 eV with a 0.5 μs shaping time. Data were collected on each of the samples with the x-ray polarization either parallel or perpendicular to the substrate surface for between 39 and 58 h.

XAFS data from a frozen solution of 5 mM YCC in 150 mM TRIS, pH 7.8 at 200 K were also collected using the 13-element germanium detector with the incident count rate kept between 30,000 and 40,000 (K. Zhang, Illinois Institute of Technology, private communication, 1998). These data were used for comparison to the monolayer data.

Optical linear dichroism measurements were recorded on the quartz/SAM/protein specimens using a Perkin-Elmer spectrophotometer (model Lambda 2, Beaconsfield, UK) over the range 350–600 nm. Only one beam was used and a rotatable polarizer was inserted before the sample cuvette (1 cm path length) so that the incident light could be polarized horizontally and vertically (in the laboratory frame). The samples were held in 1 mM TRIS buffer, pH 8.0, during the measurements to keep them fully hydrated. A cleaned, uncoated quartz slide was used to record a baseline and it was necessary to take separate baselines for the horizontal and vertical polarizations. A machined Teflon insert placed in the bottom of the cuvette was used to establish the angle of incidence of the light beam relative to the plane of the substrate, namely the plane normal at 0° or 45° to the incident beam.

RESULTS

Optical spectroscopy

Optical linear dichroism measurements were performed on the quartz/SAM/protein specimens as described above. Measurements were first taken with the incident beam perpendicular to the substrate plane to rule out any inherent dichroism in the plane of the sample. None was evident in any of the samples, as would be expected if the chromophores are azimuthally averaged about the normal to the substrate plane. Next, measurements were taken with the incident beam at 45° to the substrate plane. Four measure-

ments were taken in each polarization in a random order so as not to introduce any bias into the results. The four scans were then averaged and the horizontal and vertical polarizations compared. This procedure was repeated for four separate specimens for both the polar and nonpolar SAM surfaces. The results for one typical specimen consisting of a single monolayer of YCC on either the nonpolar SAM or the uncharged-polar SAM are shown in Fig. 1.

The dichroic ratio is defined here as the absorption with the light horizontally polarized divided by the absorption with the light vertically polarized with respect to the plane of the monolayer (or substrate). From this value, an average angle of the heme plane normal with respect to the substrate normal can be calculated as reported by Blasie et al. (1978). Using the much larger absorbance in the Soret region of the optical absorption spectrum in this case, for the YCC on the nonpolar SAMs this average heme tilt angle was calculated to be 59° ± 2°, while for the protein on the uncharged-polar SAM it was found to be 62° ± 3°. The magnitudes of the absorbances in the Soret and α band regions of the optical absorption spectra are also consistent with approximately single monolayer coverage of YCC over the surface in all of the specimens studied, using the extinction coefficients given by Dickinson and Chien (1975). Very recent polarized total internal reflection fluorescence studies of YCC, possessing a fluorescent zinc porphyrin prosthetic group, on these two different mixed endgroup SAM surfaces have also indicated rather narrow widths for the cytochrome orientational distribution in each case, as opposed to much broader widths for the pure-SH endgroup SAM surface (Tronin et al., manuscript in preparation).
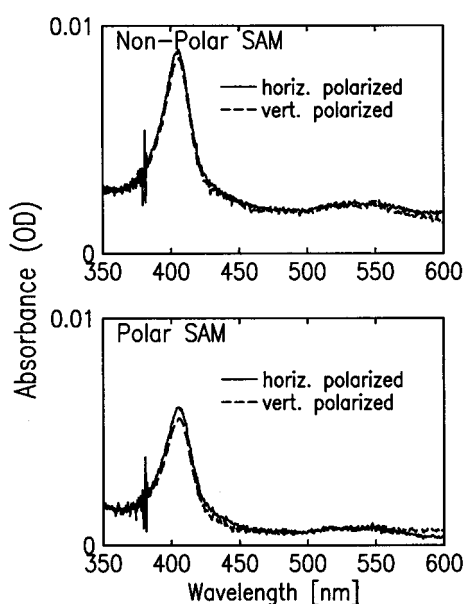

FIGURE 1 Polarized optical absorption spectra of yeast cytochrome c self-assembled onto silica substrates coated in either the nonpolar or uncharged-polar SAMs as described in the text.

Qualitative analysis of the XAFS data

Individual scans of the XAFS data were summed, then background-subtracted using a linear pre-edge function and a cubic spline for the XAFS region. The location of the wavevector $k = 0$ A^{-1} was determined by the highest peak in the derivative. The data were normalized using a fixed edge-step. This initial data reduction was performed using a PC-based version of the AT&T Bell Labs EXAFS package. There appeared to be essentially no change with time in the XAFS features or signal/noise level over the individual scans comprising each set of polarized spectra, indicating that radiation damage had been minimized (Fig. 2, a and b).

Comparing the experimental polarized XAFS data for the YCC monolayers on the nonpolar and uncharged-polar SAMs in Fig. 3, both in terms of their XAFS spectra and associated unique Fourier transforms, it is readily apparent that 1) significant polarization effects are exhibited by YCC on both SAM surfaces and 2) not only are the data significantly different from each other, but also that they are both significantly different from the unpolarized XAFS spectrum from the frozen solution of YCC shown in Fig. 4. Although only one sample of each of the two SAMs was studied by polarized XAFS due to the time restraints of these experiments, the large number of similarly prepared samples studied previously by other techniques such as optical spectroscopy and optical linear dichroism give us no reason to believe that the samples used here should be unrepresentative.

The fractional cross-section, $\chi(k)$, is given by Stern (1974), Ashley and Doniach (1975), and Lee and Pendry (1975):

$$\chi(k) = \sum_j \frac{-N_j |f_j(k, \pi)|}{kR_j^2} e^{-2\sigma_j^2 k^2} e^{-2R_j/\lambda} \sin[2kR_j + \delta_j(k)]$$

$$= -\int_0^\infty \frac{g(R)}{kR^2} \sin[2kR + \delta_j(k)] dR$$

where k is the photoelectron wave vector, N_j is the number of atoms of type j at a distance of R_j, $f_j(k, \pi)$ is the backscattering amplitude of the photoelectron from the jth atom, σ_j is the Debye-Waller factor associated with the jth atom, λ is the mean free path of the photoelectron, and $\delta_j(k)$ is the phase shift associated with the absorbing atom-backscattering atom pair, and $g(R)$ is the pair-correlation of the backscattering atoms with the absorbing atom. Thus, the fractional cross-section is simply a superposition of sine waves, the sine wave for the jth atom being weighted by two factors, one involving its backscattering amplitude as $k^{-1}|f_j(k, \pi)|$ and the other involving the iron-neighbor atom distance R_j as $R_j^{-2} \exp(-2R_j/\lambda)$, and damped by the exponential involving the Debye-Waller factor σ_j. Simply from a consideration of the partial cross-section in these terms, the differences readily evident upon comparison of the
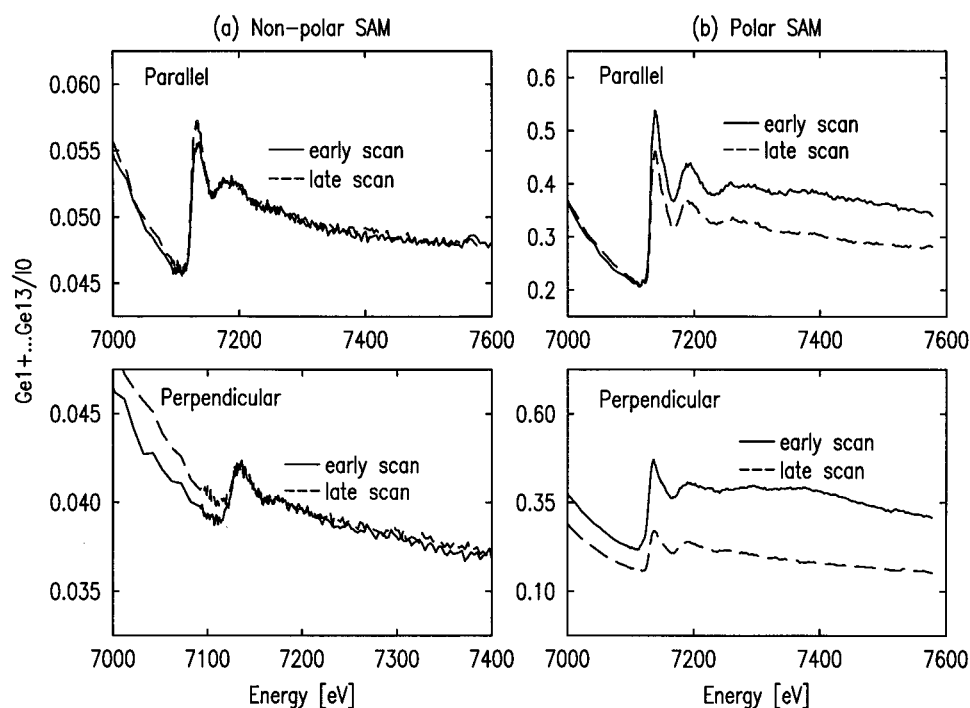
FIGURE 2   Individual scans of the XAFS "raw" data on monolayers of yeast cytochrome c taken toward the beginning and end of the data collection time for both the parallel and perpendicular polarizations on (*a*) the nonpolar SAM and (*b*) the polar SAM. [Note: the specimens were translated perpendicular to the x-ray beam while maintaining the incidence angle during the course of the individual scans for a particular polarization in order to bring unexposed portions of the monolayer into the x-ray beam to further minimize effects of radiation damage. This resulted in Bragg reflection from the substrate sometimes dominating one or more detector channels. In particular, these effects in an individual scan were either suitably minimized by small rotations of the diffractometer phi and chi angles, or the data from these channels was eliminated before further reduction and analysis. Thus, the magnitudes of the absorption edges for different individual "raw" data scans for a particular polarization can vary, as shown here.]

XAFS spectra, $k^2\chi(k)$, and their Fourier transforms, $g(R)$, described in the above paragraph also indicate, qualitatively, that either the iron atom near-neighbors are the same for all three cases (i.e., same δ_j values), but their distances R_j are somehow different, or there are differences in the nature of the iron atom near-neighbors themselves (i.e., different R_j and δ_j values), for the three different YCC environments. One might expect, at least initially, that the former case would be more likely, especially for the four pyrrol nitrogen in-plane ligands and the axial histidine nitrogen and methionine sulfur ligands in the case of YCC, which would be expected to dominate the XAFS spectra, based on the relative amplitude of the nearest-neighbor peak in the pair correlation functions. Furthermore, this qualitative comparison of the XAFS spectra for the three systems indicates that the near-neighbor environment of the heme iron atom for YCC on the nonpolar SAM surface is more similar to that of YCC in frozen aqueous solution, while that for YCC on the uncharged, polar SAM surface is less similar to that of YCC in frozen solution.

Modeling the XAFS data

Given our conclusions from the qualitative analysis of the XAFS data, together with the limited *k*-range and noise

level (especially for the perpendicular polarization) for the polarized XAFS data from these single monolayers, we decided to attempt only a limited modeling of the XAFS data in order to investigate the possible origins of the differences in the data described above. The modeling was limited in the sense that we investigated systematically only the possibility of different iron-ligand distances, i.e., iron atom first nearest-neighbor distances in-plane (all four expanded or contracted equally), and axial (expanded or contracted independently), and anisotropic nearest-neighbor motions for the three different environments of the YCC molecule.

The FEFF7.02 program (Zabinsky et al., 1995) was used to generate theoretical spectra for comparison with the experimental data. Input coordinates for FEFF7 were obtained from the NMR structural data of oxidized YCC in aqueous solution (Banci et al., 1997, serial number 1YIC) or the x-ray crystallographic data of oxidized YCC (Berghuis and Brayer, 1992, serial number 2YCC) available from the Protein Data Bank (Abola et al., 1987, 1997). This structural data set was manipulated with the molecular graphics visualization program Rasmol 2.6 (R. Sayle, Biomolecular Structures Group, Glaxo Wellcome Research and Development. Public domain source code, 1995) so that only atoms
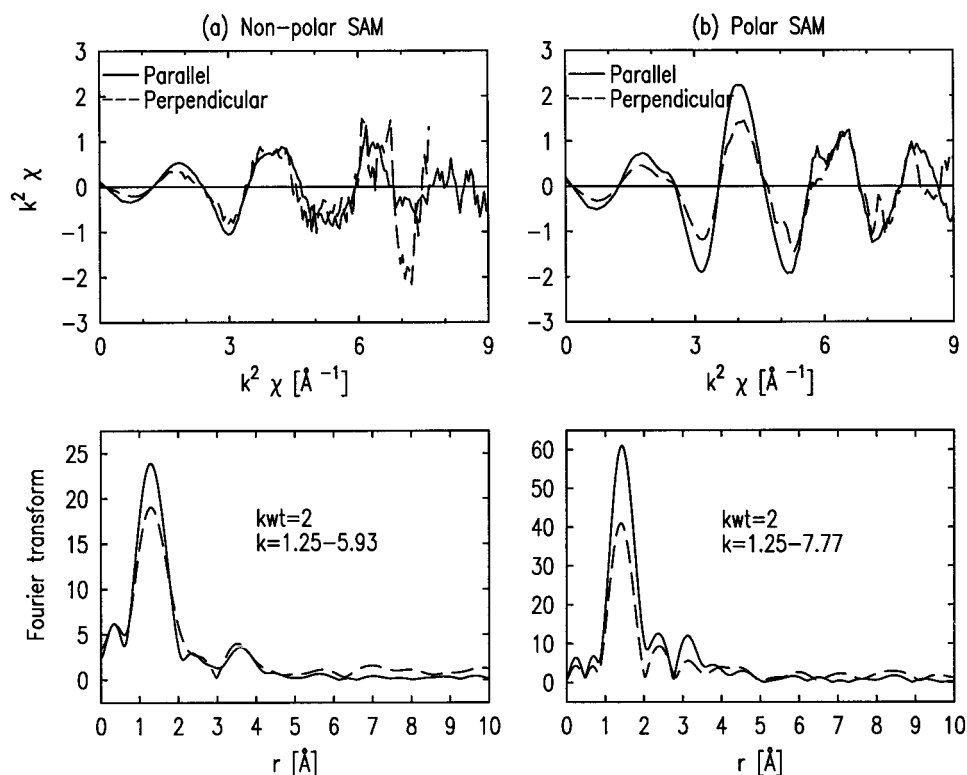
FIGURE 3 The polarized k^2-weighted experimental XAFS data and their associated Fourier transforms for monolayers of yeast cytochrome c on (*a*) the nonpolar SAM and (*b*) the polar SAM.

within a 7 Å radius from the heme iron atom were used in the model as input for FEFF7. Hydrogen atoms were excluded to reduce computational time. Using the program pdbset (CCP4, 1994), the model heme was then oriented so that its equatorial nitrogens lay in the *x-y* plane and the axial sulfur and nitrogen ligands lay approximately along the *z* axis, with the sulfur ligand along the positive *z*-direction so that the position of the cysteine 102 residue on the complete molecule would be roughly in the negative *z*-direction. The heme was then translated so that the iron atom was at the 0,0,0 coordinate position. The 7 Å radius value was chosen to allow FEFF7 to calculate accurate potentials. However, the R_{max} value in FEFF7 was set to 5 Å for all calculations (i.e., only paths with effective length up to 5 Å were included in the calculation of spectra). Initially, models based on small molecule Met-His liganded hemes were tried as input coordinates for FEFF7, but none of these gave as close a starting spectrum to the frozen solution experimental data as the heme environment from the actual protein. Using the program Autofit (Chance et al., 1996), the distances between the iron and other ligands in the starting model were then varied systematically, as described in the above paragraph; the XAFS spectrum at each distance was calculated by FEFF7 and the calculated data compared with the experimental data to give a fit index. In this way, a colored global map or grid of the fit index versus a range of any two

interatomic distances could be plotted, allowing a global minimum to be easily identified.

This approach was first applied to the unpolarized XAFS data from a frozen solution of YCC. All fits (for both the nonpolarized and polarized data) used a k^2-weighting factor. All FEFF7 calculations were performed with an amplitude reduction factor (to account for events that result in absorption, but not XAFS), $S0^2 = 0.85$. The value of NLEG in FEFF7 (number of scattering paths considered) was set to 5 since any paths larger than this were neglected by FEFF7 when using the default CRITERIA card (where any path with mean amplitude exceeding 4% of the largest path will be used in the calculation of chi). For the frozen solution of YCC, the *k*-range for fitting was 1.35–9.0 Å^{-1}. On initial comparison of the calculated spectra, the oxidized x-ray crystallographic model of YCC appeared to be the best starting point for the frozen solution data, since it already contained a shoulder on the low-*k* side of the 4 Å^{-1} peak. However, both this model and the solution NMR model were used as starting structures and both ended up producing similarly reasonable fits, as shown in Fig. 4. The iron-ligand distances, together with the estimated errors, for both fits are given in Table 1. In each case, the shoulder on the 4 Å^{-1} peak is produced by moving the sulfur ligand further away from the heme iron, though it starts at an increased distance in the x-ray model to begin with. Since fitting with
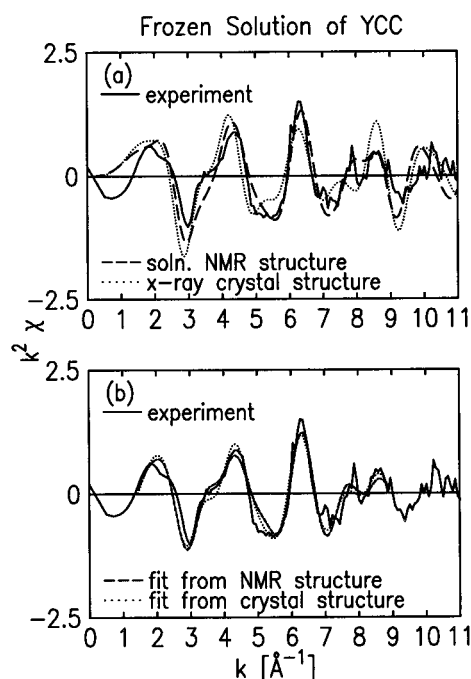
FIGURE 4 The k^2-weighted experimental XAFS data for a frozen solution of yeast cytochrome c versus (*a*) the FEFF calculated spectra from the NMR solution structure and the x-ray crystal structure, and (*b*) the best fits to the experimental data resulting from the limited modeling procedure using both the NMR solution and x-ray crystal structures as the starting models.

both models shows similar trends, it was decided to use the oxidized NMR model for the fitting of the polarized XAFS data, since this should be a better approximation to the physical form of our samples than the crystal structure.

Before the analysis of the polarized experimental XAFS data was begun, the effects of heme tilt angle and azimuthal averaging on the polarized spectra were investigated theoretically using calculated polarized XAFS spectra produced by FEFF7, using the heme model extracted from the NMR structural data. If the YCC is vectorially oriented within the monolayer by the covalent attachment of its surface cysteine to a sulfhydryl endgroup on the surface groups of the SAM, then it would be expected that the heme plane would be oriented, within a distribution of values, about some average tilt angle with respect to the substrate plane. This average heme tilt angle should then give rise to differences in the XAFS spectra of the heme iron environment with the x-ray polarization parallel versus perpendicular to the monolayer plane. However, the protein molecules are expected to be azimuthally averaged about the normal to the plane of the monolayer, while maintaining the rotational angle of the heme about its normal. The latter constraint keeps the same surface residues of the protein in contact with the SAM endgroups irrespective of the azimuthal angle. Although the effects of the heme tilt on the polarized XAFS spectra are significant both in terms of peak amplitude and position, these differences are reduced once azimuthal averaging is introduced. Fig. 5 shows the expected changes in the polarized XAFS spectra as the heme plane is varied from 30° to 75° with respect to the monolayer plane at a constant azimuthal angle. Fig. 6 shows the same representative spectra after averaging the individual spectra calculated for 0, 15, 30, 45, 60, 75, and 90° azimuthal angles for each value of the heme tilt angle. The differences between the parallel polarized spectra are markedly reduced; however, azimuthal angle does not affect the perpendicularly polarized spectra. Hence, it was necessary to include some degree of azi-

TABLE 1 Summary of possible iron-ligand bond distances, and their estimated errors, resulting from the limited modeling of the heme iron atom near-neighbor environment corresponding to the fits shown in Figs. 4, 7, and 8

Yeast Cytochrome c:	Iron-Sulfur (Å)	Iron-Axial Nitrogen (Å)	Iron-Equatorial Nitrogens (Å) (average value)
X-ray crystal structure (reduced)	2.35	1.99	1.99
X-ray crystal structure (oxidized)	2.42	2.01	2.00
NMR solution structure	2.19	1.85	2.01
Frozen solution	2.72	2.05	2.00
X-ray starting model	±0.06*	±0.06	±0.02
Frozen solution	2.69	1.92	2.03
NMR starting model	±0.025	±0.075	±0.02
On nonpolar SAM	2.25	2.79	1.99
Parallel	±0.04	±0.16	±0.04
Perpendicular	±0.2	±0.2	±0.04
On polar SAM	—†	—†	2.05

*The error analysis leading to the error estimates indicated in Table 1 was performed as outlined in Chance et al. (1996). When the fit index (the sum of the squares of the residuals between the experimental and model data) increases to Minimum Fit Index $\times$ [1 + (n_p/n_{df})] (where n_p = number of parameters used in fitting (usually 4:2 ligand distances, E0, and Debye-Waller factor), and n_{df} = number of degrees of freedom in the data based on the fitting and filtering ranges used), then the error limit is reached. This equation thus adjusts the error limits according to the number of free and fitted parameters used.
†In the case of the polar SAM, the limited modeling procedure provided most likely unphysical results for the axial ligands, and they are therefore not shown here (see Discussion).
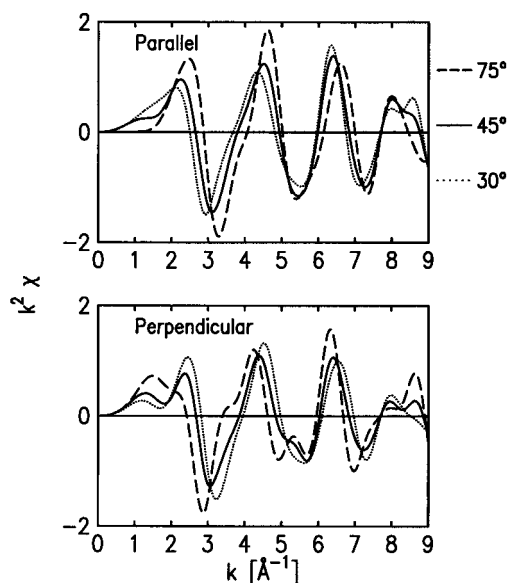
FIGURE 5   The effect of heme tilt on the polarized XAFS spectra of a monolayer of yeast cytochrome c when azimuthal averaging is not taken into account.

muthal averaging in our theoretically generated spectra to be used for comparison with the parallel polarized experimental data. Upon further investigation of the theoretically generated data, it was found that the averaging over seven azimuthal angles mentioned previously could be approximated very well by only the 45° azimuthal angle; therefore, all the comparisons made with the experimental data in the
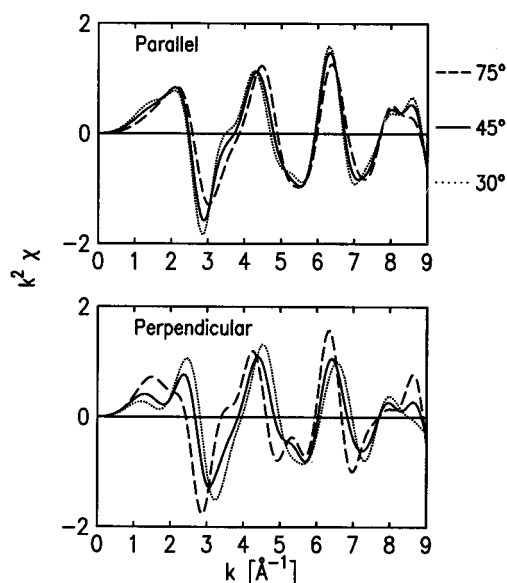

FIGURE 6   The effect of heme tilt on the polarized XAFS spectra of a monolayer of yeast cytochrome c when azimuthal averaging is taken into account.

Autofit program included this azimuthal averaging approximation in the calculated data as a substantial economy of computation time. This approximation was incorporated into the theoretically generated output by means of the polarization card in FEFF7. In other words, the polarization vector used when running Autofit was calculated to incorporate both the heme tilt and the azimuthal averaging approximation. After a reasonable fit was achieved for the parallel polarized data, the spectra could then be azimuthally averaged over a full 360°.

The experimental XAFS data and their associated Fourier transforms were shown in Fig. 3, *a* and *b* with both polarizations for the YCC on the nonpolar and uncharged-polar SAMs. In both cases, the Fourier transforms of the experimental polarized data reveal a larger first shell peak for the case with the x-ray polarization parallel to the substrate surface than for the perpendicular case, indicative of the heme plane being at a tilt-angle $>45°$ with respect to the substrate/SAM plane due to the larger backscattering amplitude of the axial sulfur ligand versus the heme in-plane nitrogens (assuming all ligands are at similar distances from the heme iron). For the calculated spectra the heme tilt-angle initially used was 60° in agreement with the experimental optical linear dichroism result, but this parameter was later varied to see whether better fits to the experimental data could be achieved. The k-range for the fits shown was 1.25–9.0 Å^{-1} and 1.25–7.0 Å^{-1} for the parallel and perpendicular spectra on the nonpolar surface and 1.25–10.8 Å^{-1} and 1.25–8.7 Å^{-1} for the parallel and perpendicular spectra on the uncharged-polar SAM.

The Autofit program allows the Debye-Waller factor and the E_0 parameter (energy at which $k = 0 \text{ Å}^{-1}$) for any calculated spectrum to be floated to minimize the fit index between the calculated spectrum and the experimental data using a nonlinear least-squares fitting program (Lee et al., 1981). Although variation of the Debye-Waller factor was allowed for initial comparisons, these values must necessarily be the same for the parallel and perpendicular polarizations of any one sample and so were later constrained to be identical for the two polarizations by means of the global Debye-Waller card, SIG2, in FEFF7. Once the best compromise between fitting of the parallel and perpendicularly polarized spectra had been achieved, heme tilt-angles either side of 60° were also investigated to see if they improved the fitting. The best fit achieved for the parallel polarization was then azimuthally averaged over 360°. In the case of the nonpolar SAM, this azimuthal averaging was performed for each of several different rotational angles of the heme about its normal, but the azimuthally averaged spectra were thereby seen to be relatively insensitive to the choice of this rotational angle.

For the nonpolar SAM, the global maps of the fit index as the iron-axial ligand distances were varied for each polarization showed only a very broad minimum rather than a clearly defined narrow minimum. Overlaying the global

maps for both the parallel and perpendicular polarized data allowed the best compromise in fitting for both polarizations to be chosen. For the parallel polarized fits, the starting fit from the NMR model had the 6.5 Å^{-1} peak in the correct position, but not the 4 Å^{-1} peak. To move this peak to the correct position and improve the fit, one axial ligand needed to move away from the heme iron by 0.85–0.95 Å and the other by 0.05–0.15 Å. However, for the perpendicularly polarized data, only moving the axial nitrogen out by ~0.94 Å and the sulfur out by ~0.06 Å produced a minimum in the global mapping, so the best compromise in fitting to both the parallel and perpendicular polarizations are the ligand distances given in Table 1, along with the estimated errors. Fitting using these interatomic distances was then performed using heme tilt-angles of 50, 55, and 65°. Improvements were made in the fit index for both the parallel and perpendicularly polarized fits for the 55° tilt. Debye-Waller factors were set to be equal for the parallel and perpendicularly polarized fits and finally, the best fits for the parallel polarization at 55° heme tilt were azimuthally averaged every 15° over 360°. This had no effect on the peak positions, but improved the fit by producing closer-fitting amplitudes. These final fits are shown in Fig. 7.

In the case of the uncharged-polar SAM, the starting fits were very different from the experimental data in terms of peak position or amplitude. Clearly defined narrow minima were obtained for both the parallel and perpendicularly polarized XAFS data by moving the axial nitrogen toward

the heme iron by around 1 Å. The fitting results are not shown in Table 1, together with the estimated errors, because the results were judged to most likely be unphysical (see Discussion for details). The Debye-Waller factors were set to be equal for the parallel and perpendicular fits and heme tilt-angles of 55 and 65° were investigated, but did not improve either the parallel or the perpendicular fits, so a tilt-angle of 60° was kept for the azimuthal averaging of the parallel fit. This resulted in a better-fitting (deeper) minimum at 3 Å^{-1}, but distorted the 6.5 Å^{-1} peak. This fit and the corresponding fit for the perpendicularly polarized data are shown in Fig. 8. For both the nonpolar and uncharged-polar SAM specimens, the in-plane nitrogens did not move from their initial positions in the starting model by >0.04 Å, as reflected in Table 1.

DISCUSSION

We expected to use the unpolarized XAFS spectrum for the frozen solution of YCC (i.e., a frozen hydrated, but isotropic environment) as a reference for the polarized XAFS spectra on the frozen hydrated single monolayers of YCC (i.e., frozen hydrated, but highly anisotropic environments). For the frozen solution of YCC, the analysis of the unpolarized XAFS data indicates that while the axial and equatorial nitrogens have moved away from the iron as compared to the NMR solution or x-ray model structures, the most significant change is in the position of the axial sulfur ligand,
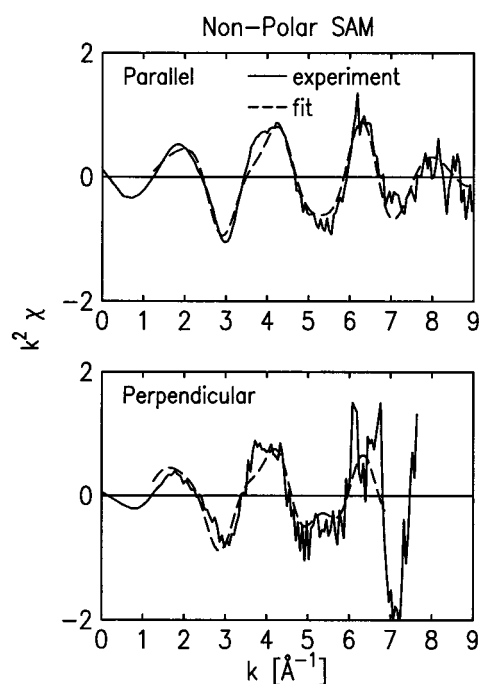

FIGURE 7 The polarized k^2-weighted experimental XAFS data for a monolayer of yeast cytochrome c on the nonpolar SAM versus the best overall fit to both polarizations after azimuthal averaging.
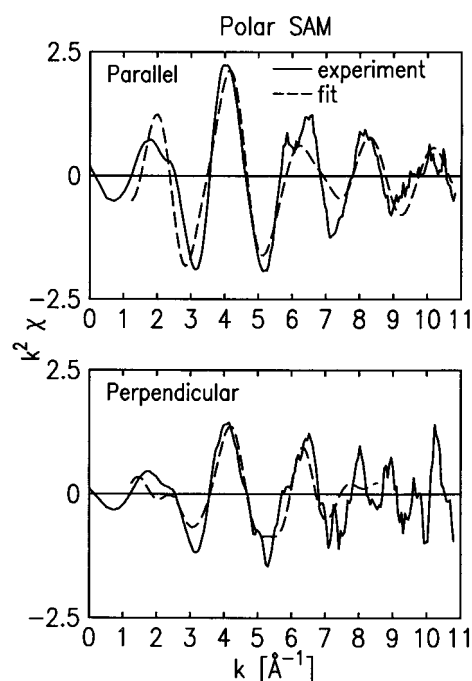

FIGURE 8 The polarized k^2-weighted experimental XAFS data for a monolayer of yeast cytochrome c on the polar SAM versus the best overall fit to both polarizations after azimuthal averaging.

which appears to have moved significantly away from the heme iron atom. Although the starting NMR model was just one of the family of 20 reported structures consistent with the solution NMR data, the average iron-sulfur value for the family was 2.25 Å, still 0.44 Å less than the best XAFS fit for the frozen solution using this model. Although other minima with shorter iron-sulfur distances were also obtained in the fitting grid, placing the axial sulfur at this greater distance from the heme iron atom was necessary to reproduce the significant shoulder on the low-k side of the maximum in the $k = 3–5$ Å^{-1} region of the XAFS spectrum (as shown by, for example, the comparison of Fig. 4 a versus 4 b).

Inasmuch as frozen dilute aqueous solutions have been generally established as the best (most functionally relevant) form of metalloproteins for structural study via the XAFS technique, the significantly longer iron-sulfur bond length for the frozen solution was somewhat unexpected. Kau et al. (1986) also used XAFS to probe the iron coordination structures in a number of ferrous porphyrin complexes containing biologically relevant sulfur donor axial ligands. Their model for the iron-methionine axial ligation provides an iron-sulfur bond length of 2.41 Å, also longer than that indicated in the NMR solution structure. The crystallographic data for other His-Met cytochrome c proteins show iron-sulfur bond lengths in the range 2.16–3.16 Å, but only from 2.21–2.43 Å restricting the spatial resolution to better than 1.8 Å. The longer iron-sulfur bond length of 2.69 Å in the frozen solution is not improbable, given that the methionine residue is known to have a poor affinity for iron and that the iron-sulfur bond of cytochrome c is generally a weak bond (Murray and Hartley, 1981). It is also possible that at this slightly alkaline pH we are beginning to see the displacement of the methionine 80 residue known to occur in cytochrome c at moderately alkaline pH values (Taler et al., 1995). The strength of the iron-sulfur bond can supposedly be probed by the weak 695-nm absorption band (Eaton and Hochstrasser, 1967), based on its polarization being normal to the heme plane, or by circular dichroism of the strong Soret band (Santucci and Ascoli, 1997), based only on the correlation of specific circular dichroism effects with the presence/absence of the 695-nm band. However, the unpolarized XAFS spectra of closely related cytochrome c's (e.g., tuna) in aqueous solution at room temperature (Korzun et al., 1982) are very similar to that reported here for the frozen aqueous solution of YCC, also containing the significant shoulder on the low-k side of the maximum in the $k = 3–5$ Å^{-1} region. But in the analysis of their XAFS data, Korzun et al. used a Fourier filtering technique, designed to isolate and thereby utilize only the first nearest-neighbor shell atoms in their fitting procedure, which resulted in removing the significant shoulder on the low-k side of the maximum in the $k = 3–5$ Å^{-1} region in the filtered spectrum. As a result, they found iron-ligand atom distances for six-coordinate irons rather close to those of the corre-sponding x-ray crystal structures and consistent with the presence of the 695-nm band more readily measured in aqueous solution. Measurement of the 695-nm band in frozen aqueous solution generally requires the presence of cryoprotective agents that were specifically not used here, e.g., 40% ethylene glycol or glycerol, in order to avoid ice microcrystal formation, which would interfere substantially with the vis-near IR spectroscopic measurements. In addition, such vis-near IR spectroscopic measurements would not be possible on the single monolayer specimens due to the very low extinction for the key 695-nm band.

The unpolarized XAFS spectrum for the frozen solution of YCC was compared with those from classical MD computer simulations in order to allow for the possibility of anisotropic motions of the iron near-neighbor atoms. MD simulations were performed initially with the coordinates for a single molecule of YCC taken from the x-ray crystal structure (Louie and Brayer, 1990, serial number 1YCC) and the six iron-ligand distances were subsequently adjusted to correspond to the XAFS fitting results to improve the starting fit due to the fact that covalent bond lengths are effected by a harmonic constraint, and therefore the mean bond length cannot change during the trajectory of a such a classical MD simulation (see below). The YCC molecule was hydrated by 500 water molecules in a 3-D MD box with periodic boundary conditions in 3-D to emulate the YCC solution (Nordgren, C. E., D. J. Tobias, M. L. Klein, and J. K. Blasie, manuscript in preparation). The iron-nitrogen bond strengths used were those based on the Raman data from myoglobin (Kuczera et al., 1990), and the iron-sulfur bond strength was approximated to be the same as the iron-axial nitrogen bond, since there were no available Raman data for this interaction, assuming here the most important aspect being that the iron and sulfur atoms were bonded, in fact, as opposed to nonbonded. The simulations were performed at 300 K using the CHARMM program, version 23 (Brooks et al., 1983) with a polar hydrogen model for the protein. Following an initial equilibration of the system for 600 ps using the YCC crystal structure coordinates, this simulation was run for an additional 200 ps with the iron-ligand distances adjusted to those from the XAFS results. All atoms within a 7 Å radius from the heme iron atom in the 20 instantaneous atomic configurations resulting from a $\Delta t = 10$ ps sampling of this 200-ps trajectory were used as input parameters in FEFF7 to generate the analogous unpolarized XAFS spectra, which were then averaged together. A global Debye-Waller factor and an E_0 shift were also used to produce the best likeness to the experimental data. The resulting calculated unpolarized XAFS spectra show a very close resemblance to the experimental spectrum (Fig. 9), but no better than those from the fitting procedure using either the x-ray crystal or solution NMR structures as the starting point (Fig. 4). The MD simulations on this system are continuing.
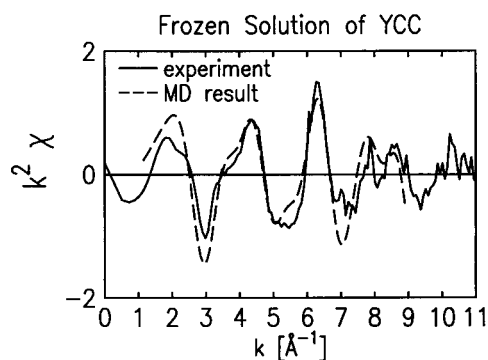
FIGURE 9   The k^2-weighted experimental XAFS data for a frozen solution of yeast cytochrome c versus the calculated XAFS spectrum generated by averaging the spectra from several instantaneous configurations of the MD computer simulation of a single, hydrated molecule of yeast cytochrome c as described in the text.

Fitting of the data from the YCC monolayer on the nonpolar SAM by iterative movement of the axial ligands resulted in extremely broad minima in the fitting grid for both the parallel and perpendicularly polarized data. The original NMR starting model structure appeared to be in one "corner" of the minima, better fits being obtained for iron-axial nitrogen and iron-sulfur distances always greater than in the starting model. The minima extended to iron-axial nitrogen and iron-sulfur distances of at least 1.5 Å above those of the model structure (fits were not extended above this value) with the deepest part of both minima occurring around iron-axial nitrogen ~ 2.79 Å and iron-sulfur ~ 2.25 Å. Moving the in-plane iron-nitrogen bond lengths in 0.02 Å from their initial values in the NMR model structure also improved the fits slightly. While the broad global minima obtained indicate that the fits are not especially sensitive to the movement of the axial ligands, better fits could only be achieved by increasing both these distances, the most significant increase being for the iron-axial nitrogen bond, and the magnitude of this increase (0.94 Å) indicates that the heme environment of the protein on the nonpolar SAM is significantly more perturbed than in the frozen solution. Varying the heme tilt-angle to 55° also improved both the fits, while a heme tilt-angle of 50° did not, indicating that the best average heme tilt-angle is somewhere between 55 and 60°, in agreement with the optical linear dichroism result of 59 ± 2°.

MD computer simulations of YCC on a nonpolar SAM used a single YCC molecule from the x-ray crystal structure covalently tethered by its surface cysteine to one sulfhydryl-terminated organic chain molecule surrounded by 95 methyl-terminated organic chain molecules, comprising a self-assembled monolayer structure, to emulate the YCC on a nonpolar SAM hydrated by 500 water molecules. The six iron-ligand distances were again adjusted to correspond to the XAFS fitting results to improve the starting model

following the initial 600-ps equilibration of the system utilizing the YCC crystal structure coordinates, and the bond-strengths used were the same as for the simulation of the YCC solution. The simulations were performed at 300 K and appropriate periodic boundary conditions were used in 3-D to model an extended monolayer system, and an all-atom model was used for the SAM. Following the initial equilibration of the system, an additional 200-ps trajectory was performed with the iron-ligand distances adjusted to those from the XAFS results, and the calculated XAFS spectra were similarly averaged over a representative number of instantaneous configurations with Debye-Waller and E_0 corrections applied as described previously. The resulting spectra for the parallel and perpendicularly polarized data are shown in Fig. 10. These averaged spectra do not appear to produce any improved match to the experimental data as compared to the XAFS fitting results shown in Fig. 7. However, following a 300-ps continuation of the initial equilibration MD trajectory performed using the unadjusted YCC x-ray crystal structure coordinates, some instantaneous configurations predicted the polarization dependence of the experimental data within the 3–5 Å^{-1} region almost to within the noise level (Fig. 11), as reported briefly elsewhere (Edwards et al., 1999), but also predicted a pronounced shoulder in the 5–6 Å^{-1} not so evident in the experimental spectra. Inspection of these instantaneous configurations indicated that out-of-plane motions for the in-
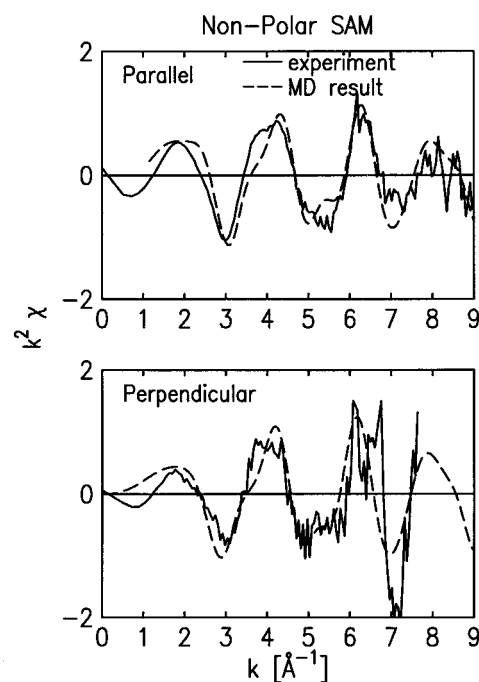

FIGURE 10   The polarized k^2-weighted experimental XAFS data for a monolayer of yeast cytochrome c on the nonpolar SAM versus the calculated spectra generated by averaging the spectra from several instantaneous configurations of the MD computer simulation on a comparable system.
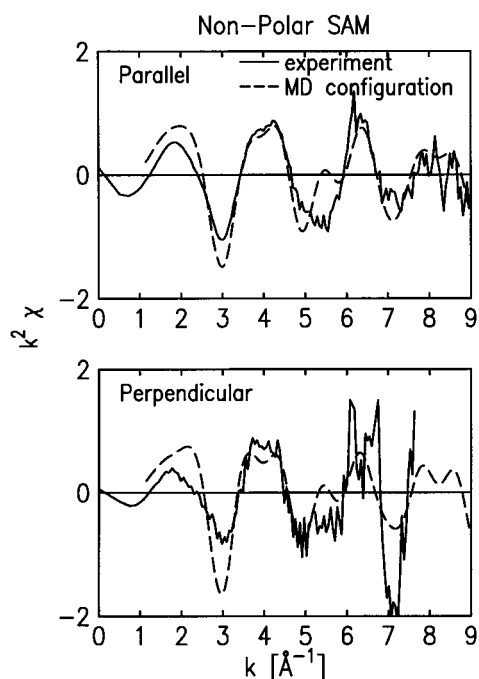
FIGURE 11 The polarized k^2-weighted experimental XAFS data for a monolayer of yeast cytochrome c on the nonpolar SAM versus the calculated spectra from one of the instantaneous configurations of the molecular dynamics computer simulation on a comparable system.
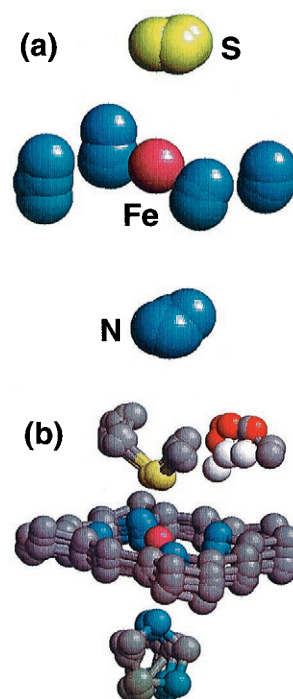

FIGURE 12 A pictorial representation of the motions experienced by (*a*) the six iron-ligands and (*b*) all atoms within 5 Å from the heme iron in YCC on a nonpolar SAM as determined from the instantaneous configurations produced by MD computer simulations. The iron atom is shown in magenta, the nitrogens in blue, carbons in gray, hydrogens in white, oxygens in red, and the sulfur atom in yellow.

plane nitrogen ligand atoms and parallel-to-the-plane motions of the axial nitrogen and sulfur ligand atoms (with respect to the heme plane) were responsible for the improvement in the shape of the spectra in the 3–5 Å^{-1} region (Fig. 12). Conversely, when the iron-ligand distances from the XAFS fitting are subsequently imposed, the 5–7 Å^{-1} region is well-fit to the data, but this almost perfect fit in the 3–5 Å^{-1} region is lost. Thus, these results may provide evidence that both iron-ligand structures occur over the YCC monolayer ensemble, as a function of either time or spatial position. The average heme angle from the additional 200-ps trajectory was 56° ± 3°, in excellent agreement with the optical linear dichroism results and the best heme tilt value returned by the XAFS fitting.

Fitting of the data from the YCC monolayer on the uncharged-polar SAM by movement of the axial ligands indicated only one significant, sharp minimum for both the parallel and perpendicular polarized data that occurred at an iron-sulfur distance of around 1.84 Å and an iron-axial nitrogen distance of around 0.85 Å. Varying the in-plane nitrogen distances resulted in a better fit if the equatorial nitrogens moved away from the heme iron 0.04 Å. No improvement in the fit was obtained by varying the heme tilt-angle to 55° or 65°, indicating that the best average heme tilt-angle is close to 60°, within the range of the optical linear dichroism result of 62 ± 3°.

The iron-nitrogen bond length of 0.85 Å provided by the XAFS data-fitting procedure described is extremely short

and most likely not physically reasonable based on the sizes of the iron and nitrogen ions/atoms. It was initially assumed that the heme ligands wouldn't be altered substantially in the monolayer, but this is evidently not the case, especially for YCC on the uncharged-polar SAM surface. Hence, the XAFS fitting procedure described that requires a fairly accurate starting model to enable relatively small changes in bond lengths to be elucidated will not be highly effective in such a case. In addition, it is evident from the MD simulations of the YCC molecule on both SAMs that the in-plane iron-ligands experience out-of-plane motion, the axial ligands experience motion parallel to the heme plane, and the heme group itself exhibits out-of-plane distortions (Fig. 12), none of which can be modeled by simply altering the bond lengths. Many other starting model structures were originally investigated and some were initially used in fitting, but the models from the NMR solution structure or the x-ray crystal structures for YCC appeared to give the most satisfactory fitting results.

MD simulations for the uncharged-polar SAM system were performed similarly to those described for the nonpolar SAM system, except the SAM was modeled as one sulfhydryl-terminated organic chain molecule tethered to a YCC molecule, and surrounded by 95 hydroxyl-terminated chains. Very poor fits to the experimental data were ob-

tained using the initial YCC crystal structure coordinates. When the iron-ligand distances were subsequently adjusted to correspond with the XAFS fitting results, the bond-strengths used would still not allow the extremely short iron-axial nitrogen distance to be reached; only when the iron-nitrogen bond-strength was also increased by an order of magnitude to approaching that of an iron-nitrogen covalent single bond did the calculated spectra begin to approach their experimental counterparts. These results, together with those described above using the XAFS fitting procedure, strongly suggest that very large forces appear to be exerted on the YCC molecule while on the polar SAM, resulting in substantial distortions of the iron-ligand structure. These distortions, including distortions away from octahedral symmetry, changes in ligand coordination species/number, etc., are too large to be effectively addressed by either the XAFS fitting procedure or the classical MD simulations used in this work.

CONCLUSIONS

In summary, the overall picture that we obtain from these first atomic-level structural measurements of the heme environment in single monolayers of yeast cytochrome c on both nonpolar and uncharged-polar soft organic surfaces is that the forces exerted on the protein by the highly anisotropic protein-SAM surface interaction are sufficient to significantly distort the iron atom near-neighbor environment in the YCC molecule as compared with an isotropic aqueous solution. The overall quality and polarization dependence of the XAFS spectra *and their respective Fourier transforms* for YCC on each of these two different soft surfaces strongly suggest that the local atomic environment within 5 Å of the heme iron atom is reasonably unique to each case. This is evident from only a qualitative analysis of the XAFS data. From the intentionally limited modeling of the XAFS data, these distortions appear to be primarily associated with the axial ligands from the protein, as one might expect. These distortions in the case of the uncharged-polar SAM are substantially greater than those for the nonpolar SAM, consistent with the qualitative comparison of their respective XAFS spectra with that for YCC in frozen aqueous solution. For the nonpolar SAM, the modeling provides a good fit to the amplitudes and positions of the major features in the experimental spectra, while the MD simulations can provide the smaller features *due to highly coupled anisotropic motions of atoms* within the iron atom's local atomic environment in the protein. For the uncharged, polar SAM, although the modeling does provide a good fit to the amplitudes and positions of the major features in the experimental spectra, the results are very unphysical, requiring an unacceptably large increase in the iron-axial nitrogen force constant in the MD simulations in order to reduce the bond length sufficiently for good agreement with the XAFS data.

We anticipate that future work using the much higher photon flux density provided by doubly focusing optics on an undulator synchrotron x-ray source, such as the Bio-CAT beamline at the Advanced Photon Source (APS), will permit us to significantly improve these initial studies by allowing data collection on more than one single monolayer specimen over a five-day period, as required in this study with a bending-magnet source. This should be especially true for the perpendicular polarization case owing to the much smaller horizontal divergence of the undulator x-ray source. Also, a new energy discriminating detector system in development will be able to use the full flux provided by such third-generation synchrotron x-ray sources. Finally, the production of long-chained, protected hydroxyl, sulfhydryl, and methyl-terminated alkylthiol compounds currently in progress will also afford the possibilities of preparing comparable nonpolar and polar SAMS on gold substrates for use in both polarized XAFS and cyclic voltammetry measurements. This would allow the direct correlation of the cytochrome heme oxidation-reduction potential with the structure of the heme iron atom's local atomic environment and provide a strong motivation for further work toward establishing the iron-ligand structure exhibited by YCC on the uncharged, polar SAM surface.

REFERENCES

Abola, E. E., F. C. Bernstein, S. H. Bryant, T. F. Koetzle, and J. Weng. 1987. Crystallographic Database-Information Content, Software Systems, Scientific Applications. F. H. Allen, G. Bergerhoff, and R. Sievers, editors. Data Commission of the International Union of Crystallography, Bonn/Cambridge/Chester. 107–132.

Abola, E. E., J. L. Sussman, J. Prilusky, and N. O. Manning. 1997. Protein data bank archives of three-dimensional macromolecular structures. *Methods Enzymol.* 277:556–571.

Ashley, C. A., and S. Doniach. 1975. Theory of extended x-ray absorption edge fine structure (EXAFS) in crystalline solids. *Phys. Rev. B: Solid State.* 11:1279–1288.

Banci, L., I. Bertini, K. L. Bren, H. B. Gray, P. Sompornpisut, and P. Turano. 1997. Solution structure of oxidized *Saccharomyces cerevisiae* iso-1-cytochrome c. *Biochemistry.* 36:8992–9001.

Berghuis, A. M., and G. D. Brayer. 1992. Oxidation state-dependent conformational changes in cytochrome c. *J. Mol. Biol.* 223:959–976.

Blasie, J. K., M. Erecinska, S. Samuels, and J. S. Leigh. 1978. The structure of a cytochrome oxidase-lipid model membrane. *Biochim. Biophys. Acta.* 501:33–52.

Blasie, J. K., S. Xu, M. Murphy, J. Chupa, J. P. McCauley, Jr., A. B. Smith III, L. J. Peticolas, and J. C. Bean. 1992. Profile structures of macromolecular monolayers on solid substrates by x-ray interferometry/holography. *Mat. Res. Soc. Symp. Proc.* 237:399–409.

Brooks, B. R., R. E. Bruccoleri, B. D. Olafson, D. J. States, S. Swaminathan, and M. Karplus. 1983. CHARMM: a program for macromolecular energy minimisation and dynamics calculations. *J. Comp. Chem.* 4:187–217.

CCP4 (Collaborative Computing Project, Number 4). 1994. The CCP4 suite: programs for protein crystallography. *Acta. Crystallogr. D.* 50: 760–763.

Chance, M. R., L. M. Miller, R. F. Fischetti, E. Scheuring, W-X. Huang, B. Sclavi, Y. Hai, and M. Sullivan. 1996. Global mapping of structural solutions provided by the extended x-ray absorption fine structure ab initio code FEFF 6.01: structure of the cryogenic photoproduct of the myoglobin-carbon monoxide complex. *Biochemistry.* 35:9014–9023.

Chupa, J. A., J. P. McCauley, Jr., R. M. Strongin, A. B. Smith III, J. K. Blasie, L. J. Peticolas, and J. C. Bean. 1994. Vectorially oriented membrane protein monolayers: profile structures via x-ray interferometry/holography. *Biophys. J.* 67:336–348.

Cullinson, J. K., F. M. Hawkridge, N. Nakashima, and S. Yoshikawa. 1994. A study of cytochrome *c* oxidase in lipid bilayer membranes on electrode surfaces. *Langmuir.* 10:877–882.

Dickinson, L. C., and J. C. W. Chien. 1975. Cobalt-cytochrome c. I. Preparation, properties and enzymic activity. *Biochemistry.* 14:3526–3534.

Eaton, W. A., and R. M. Hochstrasser. 1967. Electronic spectrum of single crystals of ferricytochrome c. *J. Chem. Phys.* 46:2533–2539.

Edmiston, P. L., J. E. Lee, S-S. Cheng, and S. S. Saavedra. 1997. Molecular orientation distributions in protein films. 1. Cytochrome c adsorbed to substrates of variable surface chemistry. *J. Am. Chem. Soc.* 119:560–570.

Edwards, A. M., J. K. Blasie, and J. C. Bean. 1998. Vectorially oriented monolayers of the cytochrome c/cytochrome oxidase bimolecular complex. *Biophys. J.* 74:1346–1357.

Edwards, A. M., J. A. Chupa, R. M. Strongin, A. B. Smith III, J. K. Blasie, and J. C. Bean. 1997. Vectorially oriented monolayers of cytochrome oxidase: fabrication and profile structures. *Langmuir.* 13:1634–1643.

Edwards, A. M., K. Zhang, C. E. Nordgren, and J. K. Blasie. 1999. Polarized XAS on vectorially oriented single monolayers of cytochrome c. Proceedings of the 10th international conference on x-ray absorption fine structure. *J. Synchrotron Radiation.* 6:411–413.

Guo, L.-H., G. McLendon, H. Razafitrimo, and Y. Gao. 1996. Photo-active and electro-active protein films prepared by reconstitution with metalloporphyrins self-assembled on gold. *J. Mater. Chem.* 6:369–374.

Jiang, M., B. Nolting, P. S. Stayton, and S. G. Sligar. 1996. Surface-linked molecular monolayers of an engineered myoglobin—structure, stability, and function. *Langmuir.* 12:1278–1283.

Kau, L-S., E. W. Svastits, M. Sono, J. H. Dawson, and K. O. Hodgson. 1986. EXAFS study of active intermediates: heme enzymes and model compounds. *Journal de Physique.* Colloque C8. Supplément au n° 12:Tome 47, Décembre, 1986.

Korzun, R., K. Moffat, K. Frank, and M. A. Cusanovich. 1982. Extended x-ray absorption fine-structure studies of cytochromes c: structural aspects of oxidation-reduction. *Biochemistry.* 21:2253–2258.

Kuczera, K., J. Kuriyan, and M. Karplus. 1990. Temperature dependence of the structure and dynamics of myoglobin. A simulation approach. *J. Mol. Biol.* 213:351–373. (See appendix and references therein.)

Lee, P. A., P. H. Citrin, P. Eisenberger, and B. M. Kincaid. 1981. Extended x-ray absorption fine structure: its strengths and limitations as a structural tool. *Rev. Mod. Physics.* 53:769–806.

Lee, P. A., and J. B. Pendry. 1975. Theory of the extended x-ray absorption fine structure. *Phys. Rev. B: Solid State.* 11:2795–2811.

Louie, G. V., and G. D. Brayer. 1990. High-resolution refinement of yeast iso-1-cytochrome c and comparisons with other eukaryotic cytochromes c. *J. Mol. Biol.* 214:527–555.

Murray, S. G., and F. R. Hartley. 1981. Coordination chemistry of thioethers, selenoethers, and telluroethers in transition-metal complexes. *Chem. Rev.* 81:365–414.

Owaku, K., M. Goto, Y. Ikariyama, and M. Aizawa. 1995. Protein A Langmuir-Blodgett film for antibody immobilization and its use in optical immunosensing. *Anal. Chem.* 67:1613–1616.

Pachence, J. M., S. Amador, G. Maniara, J. Vanderkooi, P. L. Dutton, and J. K. Blasie. 1990. Orientation and lateral mobility of cytochrome *c* on the surface of ultrathin lipid multilayer films. *Biophys. J.* 58:379–389.

Pachence, J. M., and J. K. Blasie. 1987. The location of cytochrome c on the surface of ultrathin lipid multilayer films using x-ray diffraction. *Biophys. J.* 52:735–747.

Pachence, J. M., R. F. Fischetti, and J. K. Blasie. 1989. Location of the heme-iron atoms within the profile structure of a monolayer of cytochrome *c* bound to the surface of an ultrathin lipid multilayer film. *Biophys. J.* 56:327–337.

Sagiv, J. 1980. Organized monolayers by adsorption. I. Formation and structure of oleophobic mixed monolayers on solid surfaces. *J. Am. Chem. Soc.* 102:92–98.

Santucci, R., and F. Ascoli. 1997. The Soret circular dichroism spectrum as a probe for the heme Fe(III)-Met(80) axial bond in horse cytochrome c. *J. Inorg. Biochem.* 68:211–214.

Song, S., R. A. Clark, E. F. Bowden, and M. J. Tarlov. 1993. Characterization of cytochrome *c*/alkanethiolate structures prepared by self-assembly on gold. *J. Phys. Chem.* 97:6564–6572.

Stern, E. A. 1974. Theory of the extended x-ray absorption fine structure. *Phys. Rev. B: Solid State* 10:3027–3037.

Taler, G., A. Schejter, G. Navon, I. Vig, and E. Margoliash. 1995. The nature of the thermal equilibrium affecting the iron coordination of ferric cytochrome c. *Biochemistry.* 34:14209–14212.

Wasserman, S. R., H. Biebuyck, and G. M. Whitesides. 1989. Monolayers of 11-trichlorosilylundecyl thioacetate: a system that promotes adhesion between silicon dioxide and evaporated gold. *J. Mater. Res.* 4:886–892.

Xu, S., R. F. Fischetti, J. K. Blasie, L. J. Peticolas, and J. C. Bean. 1993. Profile and in-plane structures of self-assembled monolayers on Ge/Si multilayer substrates by high-resolution x-ray diffraction employing x-ray interferometry/holography. *J. Phys. Chem.* 97:1961–1969.

Zabinsky, S. I., J. J. Rehr, A. Ankudinov, R. C. Albers, and M. J. Eller. 1995. Multiple-scattering calculations of x-ray absorption spectra. *Phys. Rev. B.* 52:2995–3009.

Zhang, K., A. M. Edwards, J. Dong, J. Chupa, and J. K. Blasie. 1997. XAFS on Vectorially oriented single monolayer protein samples. *J. Phys. IV France* 7:Colloque C2. Supplément au Journal de Physique III d'avril, 1997. C2:593–597.